DTIC FILE COPY

AGARD-CP-454

AGARD-CP-454

AGARD

ADVISORY GROUP FOR AEROSPACE RESEARCH & DEVELOPMENT

7 RUE ANCELLE 92200 NEUILLY SUR SEINE FRANCE

AD-A221 594

AGARD CONFERENCE PROCEEDINGS No.454

Atmospheric Propagation in the UV, Visible, IR and MM-Wave Region and Related Systems Aspects

This Document Reproduced From Best Available Copy

DTIC ELECTE MAY 17 1990 S E D

DISTRIBUTION STATEMENT A

Approved for public release; Distribution Unlimited

NORTH ATLANTIC TREATY ORGANIZATION

DISTRIBUTION AND AVAILABILITY ON BACK COVER

90 05 16 198

AGARD-CP-454

NORTH ATLANTIC TREATY ORGANIZATION

ADVISORY GROUP FOR AEROSPACE RESEARCH AND DEVELOPMENT

(ORGANISATION DU TRAITE DE L'ATLANTIQUE NORD)

DTIC COPY INSPECTED

AGARD Conference Proceedings No.454

ATMOSPHERIC PROPAGATION IN THE UV, VISIBLE, IR AND MM-WAVE REGION AND RELATED SYSTEMS ASPECTS

Accession For
NTIS CRA&I ☒
DTIC TAB ☐
Unannounced ☐
Justification
By
Distribution/
Availability Codes
Dist | Avail and/or Special
A-1

Papers presented at the Electromagnetic Wave Propagation Panel Specialists' Meeting, held in Copenhagen, Denmark, 9th—13th October 1989

THE MISSION OF AGARD

According to its Charter, the mission of AGARD is to bring together the leading personalities of the NATO nations in the fields of science and technology relating to aerospace for the following purposes:

- Recommending effective ways for the member nations to use their research and development capabilities for the common benefit of the NATO community;
- Providing scientific and technical advice and assistance to the Military Committee in the field of aerospace research and development (with particular regard to its military application);
- Continuously stimulating advances in the aerospace sciences relevant to strengthening the common defence posture;
- Improving the co-operation among member nations in aerospace research and development;
- Exchange of scientific and technical information;
- Providing assistance to member nations for the purpose of increasing their scientific and technical potential;
- Rendering scientific and technical assistance, as requested, to other NATO bodies and to member nations in connection with research and development problems in the aerospace field.

The highest authority within AGARD is the National Delegates Board consisting of officially appointed senior representatives from each member nation. The mission of AGARD is carried out through the Panels which are composed of experts appointed by the National Delegates, the Consultant and Exchange Programme and the Aerospace Applications Studies Programme. The results of AGARD work are reported to the member nations and the NATO Authorities through the AGARD series of publications of which this is one.

Participation in AGARD activities is by invitation only and is normally limited to citizens of the NATO nations.

The content of this publication has been reproduced
directly from material supplied by AGARD or the authors.

Published March 1990

Copyright © AGARD 1990
All Rights Reserved

ISBN 92-835-0548-4

Printed by Specialised Printing Services Limited
40 Chigwell Lane, Loughton, Essex IG10 3TZ

THEME

Atmospheric propagation of electromagnetic waves at frequencies above 30 GHz, i.e. millimeter (MM) waves and infra-red (IR), visible and to some extent also ultra-violet (UV) radiation, is of importance to many current and future military applications. Propagation phenomena affect and often limit navigation, communications, surveillance, search, target acquisition, fire control, autonomous weapons guidance, kill assessment, countermeasures and medium to high power laser applications.

Recent advances in components and technology have prompted extensive studies and novel applications in the above wavelength region. Specifically, second generation infra-red detector technology, smart image processing, as well as active coherent detection systems, i.e. millimeter wave and laser radars, have required dedicated propagation studies, including much longer ranges over land and sea, multiple scattering effects and especially turbulence induced systems limitations.

An exchange of information between scientists and engineers involved in research and development in this wavelength region will benefit further development of systems and explore new areas of research as well as military and civilian applications. The following topics were discussed:

1 — Propagation measurements;
2 — Propagation models;
3 — Sensing of the propagation environment;
4 — System aspects and performance modelling;
5 — Countermeasures.

The term propagation included atmospheric absorption, scattering, path radiance effects, turbulence effects and blooming, as created by the ambient atmosphere and by the battle-field effects. The term sensing covered in-situ as well as remote techniques. Systems performance modelling and countermeasures concentrated on topics which are directly related to those propagation effects.

* * *

La propagation des ondes électromagnétiques à des fréquences supérieures à 30 GHz, c'est à dire les ondes millimétriques (MM) et l'infrarouge (IR), les rayonnements visibles et dans une certaine mesure ultra-violets, a de l'importance pour bon nombre d'applications militaires actuelles et futures. Les phénomènes de propagation ont une influence qui est souvent limitative sur la navigation, les télécommunications, la surveillance, la détection, l'acquisition de la cible, la conduite de tir, le guidage des missiles autonomes, les prévisions de destruction, les contremesures et les applications des lasers de moyenne à haute puissance.

Les progrès réalisés dernièrement dans le domaine de la technologie des composants ont amené des études importantes, lesquelles ont débouché sur des applications novatrices dans la gamme de fréquence citée ci-dessus. En particulier, la technologie de la deuxième génération des capteurs infra-rouges, le traitement intelligent des images ainsi que les systèmes actifs de détection cohérente, c'est à dire les radars à laser et les radars à ondes millimétriques, ont éxigé la réalisation d'études spécifiques à la propagation, qui tiennent compte de portée beaucoup plus grandes au-dessus de la terre et de la mer, des effets multiples de diffusion et les limitations imposées aux systèmes par la turbulence atmosphérique.

Un échange d'informations entre les scientifiques et ingénieurs travaillant dans ce domaine favorise le développement ultérieur des systèmes en question tout en permettant d'examiner de nouvelles possibilités de recherche et des applications civiles et militaires. Les sujets suivants furent abordés:

1 — La mesure de la propagation;
2 — La modélisation de la propagation;
3 — La détection du milieu de propagation;
4 — Les aspects des systèmes et la modélisation des performances;
5 — Les contremesures.

Le terme "propagation" comprend les notions suivantes, l'absorption atmosphérique, la diffusion, les effets de la luminance énergétique selon le parcours, les effets de la turbulence et l'efflorescence, créés par l'atmosphère ambiante et par les effets du champs de bataille.

Le terme "détection" comprend ici les techniques de détection in situ aussi bien que la télédétection. La modélisation des performances de systèmes et les contremesures concernent principalement des sujets ayant un rapport direct avec les effets de la propagation cités plus haut.

ELECTROMAGNETIC WAVE PROPAGATION PANEL OFFICERS

Chairman: Prof. C.Goutelard
Directeur LETTI
Université Paris-Sud
9, Avenue de la Division Leclerc
94230 Cachan
France

Deputy Chairman: Ir H.Vissinga
van Kempenstraat 30
2252 VH Voorschoten
Netherlands

TECHNICAL PROGRAMME COMMITTEE

CHAIRMEN

Dr D.Höhn
Direktor, Forschungsinstitut für Optik
Schloß Kreßbach
D-7400 Tübingen
Federal Republic of Germany

Dr J.H.Richter
Head, Ocean and Atmospheric Sciences Division
Naval Ocean Systems Center
Code 54
San Diego, 92152-5000
United States

MEMBERS

Prof. Dr J.B.Andersen
Institut for Elektronische Systemer
Aalborg Universitet
DK-9000 Aalborg
Denmark

Dr J.E.A.Selby
Grumman Corporate Research Center
MS — AO8 — 35
S. Oyster Bay Road
Bethpage, NY 11714
United States

Dr J.Fritz
ONERA
BP 72
92322 Chatillon Cedex
France

Dr F.E.Niles
Atmospheric Sciences Laboratory
White Sands Missile Range
NM 88002-5501
United States

Dr H.M.Lamberton
Royal Signal and Radar Establishment
EM1
Malvern Worcs WR14 3PS
United Kingdom

Dr P.L.Roney
Defence Research Establishment
Valcartier
PO Box 8800
Courcelette, Quebec GOA 1RO
Canada

Dr C.W.Lamberts
Physics and Electronics Laboratory
TNO, (Physics Group)
Oude Waalsdorperweg 63
2597 AK Den Haag
Netherlands

ELECTROMAGNETIC WAVE PROPAGATION PANEL EXECUTIVE

From Europe
L. Col. P.A.Brunelli
AGARD — EPP Executive
7, rue Ancelle
92200 Neuilly sur Seine
France

From USA and Canada
AGARD — NATO
ATTN: EPP Executive
APO New York 09777

CONTENTS

* Printed in classified publication CP454 (Supplement).

* Printed in classified publication CP454 (Supplement).

PREFACE

With the symposium "Atmospheric Propagation in the UV, Visible, IR and MM-wave Region and Related Systems Aspects", the AGARD Electromagnetic Wave Propagation Panel (EPP) adhered to its practice of periodically reviewing the recent advances in this technical area. This field is still expanding and is of great importance to the development of modern systems and their most effective application. Atmospheric propagation is crucial to the performance of all systems operating from the UV to the MM-wave region because it limits their operational ranges, which depend on the prevailing environmental conditions and their history. In other cases, propagation effects permit specific applications, e.g., warning devices based on scattered radiation. The importance of such a symposium was already evident shortly after the call for papers by the large number of very appropriate contributions. The result was a stimulating meeting at Copenhagen, Denmark, 9—13 October 1989. The Conference proceedings contain all papers and following discussions. Volume one deals with the unclassified portion and volume two with the classified session of the meeting.

The contributions have shown, that within the last decade many atmospheric propagation problems relevant to electro-optical and laser systems, including battlefield effects, have been investigated experimentally and theoretically with such a quality, that quite sophisticated propagation codes and systems performance models are available for both armament oriented systems analyses and development of tactical decision aids. The symposium has also pointed out that still-developing, electro-optical and MM-wave technologies require additional, complex, propagation research efforts and studies for operationally-relevant systems performance analyses.

The following areas were identified as requiring future research:

— Transfer of information/images through the atmosphere in addition to studies related to the basic effects, such as emission, absorption, scattering, refraction and turbulence.

— Effects of complex backgrounds, e.g., atmospheric emission, specific cloud patterns, properties of the sea-air-environment.

— Propagation effects related to UV-applications.

— Propagation effects related to high power laser beams.

— Propagation and background effects related to space-to-ground observation tasks, in addition to the ground-to-ground and air-to-ground/ground-to-air scenarios over land and sea.

— Effects within optically dense media, e.g., multiple-scattering effects in clouds and smogs.

The above areas were either specifically addressed by contributions, or they were identified during the course of the presentations and discussions.

In summary, the symposium provided the intended review on the state-of-the-art in this field of systems-oriented atmospheric research, discussed experimental, modelling and theoretical aspects, and indicated clearly the most essential areas of current and future defence-oriented atmospheric research related to UV, visual, IR and MM-wave-systems.

Gratefully acknowledged are the cooperation and assistance received by the members of the Programme Committee and the session chairmen: Prof. Dr J.B.Andersen, Dr J.Fritz, Mr F.Christophe, Dr H.M.Lamberton, Dr. C.W.Lamberts, Dr F.E.Niles, Dr P.L.Roney and Dr J.E.A.Selby.

Appreciation is furthermore expressed to all who helped in the organization of the symposium and in the compilation of the Proceedings, to authors and contributors to discussions, to the host coordinators, to the AGARD staff, especially the EPP executive, Lt Col. P.A.Brunelli.

D.H.Höhn and J.H.Richter
Co-chairmen and editors

MODELING MILLIMETER-WAVE PROPAGATION EFFECTS IN THE ATMOSPHERE

H. J. Liebe and G. A. Hufford

National Telecommunications and Information Administration
Institute for Telecommunication Sciences
325 Broadway
Boulder, CO 80303, U.S.A.

SUMMARY

Two millimeter-wave propagation models, called MPM and MZM, are discussed. The first one predicts, at frequencies up to 1000 GHz, loss and delay effects for a nonprecipitating atmosphere. Contributions from dry air and water vapor are addressed, as well as suspended water droplets that simulate fog or cloud conditions. For clear air, a local spectral line base is employed (44 O_2 + 30 H_2O lines) complemented by an empirical water-vapor continuum. Droplet effects are treated with the approximate Rayleigh scattering theory. Input variables are barometric pressure, temperature, relative humidity, and droplet concentration.

At heights between 30 and 100 km, the spectral lines of oxygen result in an anisotropic medium due to the geomagnetic Zeeman effect. The computer program MZM was developed to analyze propagation of plane, polarized radio waves in the vicinity (±10 MHz) of O_2 line centers positioned in the 60-GHz band and at 119 GHz. Results are displayed that demonstrate many aspects of the unusual wave propagation through the mesosphere.

1. INTRODUCTION

The parameters of a radio wave are modified on propagation through the atmosphere. In general, such influences are due to refraction, absorption, and scatter. The complex refractive index, $n = n' + in''$, is a measure of the interaction of electromagnetic radiation with the medium and depends on frequency and atmospheric conditions. Its real part, n', exceeds unity by a small amount ($n' - 1 \leq 0.0004$), slowing the propagation velocity to values less than speed of light in vacuum, while the positive imaginary part (n'') pertains to a loss of wave energy.

Complex refractivity, expressed in units of parts per million,

$$N = (n - 1)10^6 = N_0 + N'(f) + iN''(f) \quad \text{ppm,} \tag{1}$$

is a sensible measure of electromagnetic properties exhibited by the atmosphere. Frequency-independent contributions, N_0, and respective refraction and absorption spectra, $N'(f)$ and $N''(f)$, can be specified.

Refractivity N is the center piece of models that characterize atmospheric radio-wave propagation. Two methods are discussed here to compute refractivity: In MPM, the standard case of an isotropic medium is dealt with [1]; on the other hand, in MZM a very special case is treated where, in the mesosphere, the medium behaves anisotropically and wave transmission depends on location, direction, and polarization [2].

1.1 Standard Atmospheric Propagation (MPM)

Free propagation of a plane wave in the z-direction is described by

$$E(z) = \exp[ikz(1 + N)]\, E_0 \tag{2}$$

where $E(z)$ is the electric field strength at a distance z along the path, which may be curved by refractive gradients $Re(dN/dz)$ according to *Snell*'s law; $E_0 = E(z = 0)$ is the initial value; $k = 2\pi f/c$ is the free space wave number, and c is the speed of light in vacuum. Assuming the units for frequency f in GHz and for refractivity N in ppm, we have in more practical terminology the dispersive propagation rates of power attenuation α and phase lag β (or delay time τ); that is,

$$\alpha = 0.1820\, f\, N''(f) \quad \text{dB/km}$$

and

$$\beta = 1.2008\, f\, N'(f) \quad \text{deg/km , or} \tag{3}$$
$$\tau = 3.3356\, N'(f) \quad \text{ps/km ,}$$

where $0.1820 = (4\pi/c)10 \cdot \log e$, $1.2008 = (2\pi/c)(180/\pi)$, and $3.3356 = 1/c$.

Program MPM has five modules: (a) nondispersive refractivity N_0, (b) contributions from 44 O_2 and 30 H_2O local (≤ 1 THz) line spectra, (c) the nonresonant dry air spectrum, (d) an empirical water vapor continuum that reconciles discrepancies with experimental absorption results, and (e) a refractivity due to suspended water droplets. Two additional modules estimate haze (i.e., reversible swelling or shrinking of hygroscopic aerosols when relative humidity varies between 80 and 99.9 %) and rain effects [1], but are not discussed here.

Section 2 gives the particulars how to compute refractivity N from five input parameters:

frequency	f	1 - 1000	GHz,	
barometric (total) pressure	P	110 - 10^{-5}	kPa,	
temperature	T	-60 - 50	°C,	(4)
relative humidity	U	0 - 100	%RH,	and
suspended water droplet concentr. at 100 %RH	W	0 - 5	g/m^3.	

The spatial distribution of these variables along a radio path specifies an inhomogeneous propagation medium [3], a case not treated here. The O_2 *Zeeman* effect is approximated in MPM so that the height range can be extended to 100 km, but trace gas spectra (O_3, CO, N_2O, ClO, etc.) are missing.

1.2 Anisotropic Propagation In The Mesosphere (MZM)

At high-altitude (30 - 100 km) pressures, the O_2 lines appear as isolated features and their spectral signature is governed by the *Zeeman* effect due to the geomagnetic field. The magnetic flux density B_0 varies with location and height and splits each line into three groups of Zeeman components [see (20)] that are spread, proportional to B_0, over a range of a few megahertz. The spatial dependenceof these three groups leads to anisotropic interactions with an electromagnetic field.

Following (2), the propagation of a plane, polarized wave is formulated by

$$\underline{E}(z) = \exp[ikz(I_2 + N_2)]\,\underline{E}_0\ , \tag{5}$$

where z is the distance along a straight-line path. For the x/y-plane of polarization (orthogonal to z) we define $\underline{E}(z)$, a two-dimensional field vector; $\underline{E}_0 = \underline{E}(z=0)$, the initial value; I_2, the 2x2 unit matrix; and N_2, a 2x2 refractivity matrix. Analysis of the complex field $\underline{E}$ implies a shorthand notation for $Re[\exp(-i2\pi ft)\ \underline{E}]$. As the time t increases through one cycle, this real vector describes an "ellipse of polarization". The program MZM was developed [2] to solve (5) for a spherically stratified mesosphere (i.e., concentric height intervals of 1 km between 30 and 100 km [13]) as detailed in Section 3.

2. THE MPM MODEL

The concept of an atmospheric millimeter-wave propagation model in the form of N(f) was introduced in [3]. Modular, quantitative relationships correlate meteorological conditions encountered in the neutral atmosphere with refractivity formulations. Contributions by dry air, water vapor, and suspended water droplets (haze, fog, cloud) are covered in [1]. Refractivity of air can be obtained, in principle, by considering all known resonant, far-wing, and nonresonant radio-wave interactions with the matter in a given volume element. Various degrees of approximations have been employed to reduce labor and computer time, as well as to bridge unknown spectroscopic information.

2.1 Atmospheric Model Parameters

Atmospheric input parameters are converted into internal model variables; that is, temperature T (°C) into a relative inverse temperature variable

$$\theta = 300/(T + 273.15); \tag{6}$$

and relative humidity into

$$U = (e/e_s)100 \le 100 \qquad \%RH\ , \tag{7}$$

whereby the temperature dependence of the water vapor saturation pressure e_s (100 %RH) is approximated, and in turn, expressed as vapor pressure e or concentration v; i.e.,

$$\begin{aligned} e &= 2.408\cdot 10^8\ U\ \theta^4 \exp(-22.64\ \theta) && \text{kPa} \\ v &= 7.223\ e\ \theta && \text{g/m}^3\ . \end{aligned} \tag{8}$$

Equation (8) allow one to correlate relative (U) and absolute (e or v) humidity and thus to separate tho total pressure into partial pressures for dry air and water vapor (P = p + e).

Suspended water droplets representing fog or cloud conditions are described by a water droplet concentration W, which can be deduced from measured drop size spectra or estimated as path-average from optical visibility data. Cloud coverage is a frequent event that typically occurs half of the time with vertical extensions of up to 2 km. Whenever a concentration W is considered in MPM [i.e., (9) and (15)], the relative humidity has to be set to U = 100 % ($e = e_s$).

2.2 Complex Refractivity

The total complex refractivity in MPM consists of nondispersive and dispersive parts, $N_t = N_o + N(f)$. Nondispersive refractivity is terms of $P = p + e(U)$, θ, and W follows from

$$N_o = [2.589p + (41.63\theta + 2.39)e]\theta + W[1.5 - 4.5/(\epsilon_s + 2)]\ , \tag{9}$$

with $\epsilon_s = 77.66 + 103.3(\theta - 1)$ being the static permittivity of liquid water (see equation 16).

Dispersive complex refractivity is assumed to be the sum of four contributions,

$$N(f) = N_L(f) + N_D(f) + N_V(f) + N_W(f), \tag{10}$$

where N_L represents local (≤ 1 THz) line contributions,
N_D and N_V are dry air and water vapor continuum spectra, and
N_W is the refractivity spectrum due to suspended water droplets.

2.3 Local Line Absorption and Dispersion

A line-by-line summation of local spectra by the two principle absorber molecules, O_2 and H_2O, yields the the refractivity contribution

$$N_L = \sum_{j=1}^{44} S_j F_j(f) + \sum_{k=1}^{30} S_k F_k(f) \quad , \qquad (11)$$

where S is a line strength in kHz, $F = F' + iF''$ is a complex shape function in GHz^{-1}, and j,k are the line indices. The Van Vleck-Weisskopf shape function, modified by Rosenkranz [5],[6] to include pressure-induced line interference, was selected to describe line broadening as follows:

$$F(f) = (f/\nu_0)[(1 - i\delta)/(\nu_0 - f - i\gamma) \; - \; (1 + i\delta)/(\nu_0 + f + i\gamma)] \qquad (12)$$

defining dispersion [$Re\ F = F'(f)$] and absorption [$Im\ F = F''(f)$] spectra [1], and the parameters are:

	Symbol	O_2 Lines in Air (j)	H_2O Lines in Air (k)	
strength	S, kHz	$a_1 10^{-6} p\theta^3 \exp[a_2(1 - \theta)]$	$b_1 e\theta^{3.5} \exp[b_2(1 - \theta)]$	(12a)
width	γ, GHz	$a_3 10^{-3}(p\theta^{(0.8 - a_4)} + 1.1e\theta)$	$b_3 10^{-3}(p\theta^{b_4} + b_5 e\theta^{b_6})$	(12b)
interference	δ	$(a_5 + a_6\theta)10^{-3} p\theta^{0.8}$	0	(12c)

A current set of line center frequencies ν_0 and spectroscopic coefficients a_1 to a_6 and b_1 to b_6 for strength S, pressure-broadened width γ and interference δ is given in Table 1 of reference [1]. The computing efficiency of MPM can be improved by approximating the temperature dependence of the width of water vapor lines by setting summarily $b_4 \approx 0.7$ and $b_6 \approx 0.9$.

Zeeman-splitting of O_2 lines has to be taken into account for altitudes above 30 km. Model MZM was developed to treat this special problem (see Section 3). A rough estimate of oxygen line behavior in the mesosphere is made in MPM by replacing the widths γ_j (12b) with

$$\gamma_j^h \approx [\gamma_j^2 + (25 \cdot B_0)^2]^{1/2} \qquad \text{GHz} \; , \qquad (12d)$$

where the geomagnetic flux density B_0 is in microtesla (μT). Doppler-broadening of H_2O lines at heights above 50 km is considered by substituting the widths γ_k with (ν_0 in GHz)

$$\gamma_k^h \approx [\gamma_k^2 + 2.14 \cdot 10^{-12} \nu_{0,k}^2/\theta]^{1/2} \qquad \text{GHz} \; . \qquad (12e)$$

2.4 Nonresonant Dry Air Spectrum

Nonresonant refractivity terms of dry air make a small contribution [3],

$$N_D(f) = S_d(1/[1 - i(f/\gamma_d)] - 1) + iN_p'' , \qquad (13)$$

due to the O_2 Debye spectrum, $S_d = 6.14 \cdot 10^{-4} p\theta^2$ (kHz) and $\gamma_d = 5.6 \cdot 10^{-3}(p + 1.1e)\theta^{1.05}$ (GHz) [4],

and pressure-induced nitrogen absorption, $N_p'' = 1.40 \cdot 10^{-10} f(1 - 1.2 \cdot 10^{-5} f^{1.5}) p^2 \theta^{3.5}$.

2.5 Water-Vapor Continuum

The real part of the water-vapor continuum spectrum, N_V', is a theoretical estimate, while the loss term, N_V'', is an empirical formulation leading to [1]

$$N_V'(f) \approx f^2(1 - 0.20 \cdot \theta)e\theta^3 10^{-5} \quad \text{and} \quad N_V''(f) \approx f(b_e e + b_p p)e\theta^3 10^{-5} \; , \qquad (14)$$

where $b_e = 3.57 \cdot \theta^{7.5}$ and $b_p = 0.113$. Equation (14) supplements the H_2O line contribution $N_{L,k}$ (11).

Experimental attenuation rates α_x of moist air generally exhibit more water-vapor absorption than is contributed by the H_2O line base. The excess is most pronounced in atmospheric millimeter-wave window ranges. Continuum absorption N_V'' was determined by a series of accurate laboratory measurements in the 140-GHz window range where absolute attenuation $\alpha_x(P,T,U)$ was measured at f_x = 138 GHz for both pure water vapor and moist air conditions [7]. The b_e-term of (14) with its strong negative temperature dependence, so far, has not found a sound theoretical explanation. Hypotheses about its origin consider wing contributions from self-broadened H_2O lines above 1 THz, collision-induced absorption, and water dimers. These three effects may be involved separately or collectively [6].

2.6 Suspended Water Droplet Refractivity

Suspended water droplets in fogs or clouds are efficient millimeter-wave absorbers. Their maximum radii are below 50 μm, which allows the approximate Rayleigh scattering theory to be applied to formulate complex refractivity contributions [8],

$$N_W(f) = W[1.5 - 4.5/(\epsilon + 2)] \; . \qquad (15)$$

The complex permittivity spectrum of liquid water, ϵ, is given up to 1000 GHz by a double-Debye model,

$$\epsilon(f) = (\epsilon_s - \epsilon_1)/[1 - i(f/f_{D1})] + (\epsilon_1 - \epsilon_2)/[1 - i(f/f_{D2})] + \epsilon_2 \; , \qquad (16)$$

where ϵ_s is given at equation (9); the high frequency constants are $\epsilon_1 = 5.48$ and $\epsilon_2 = 3.51$, and the two relaxation frequencies are (in GHz)

$$f_{D1} = 20.09 - 142(\theta - 1) + 294(\theta - 1)^2 \qquad \text{and}$$

$$f_{D2} = 590 - 1500(\theta - 1) \; .$$

N"

N'

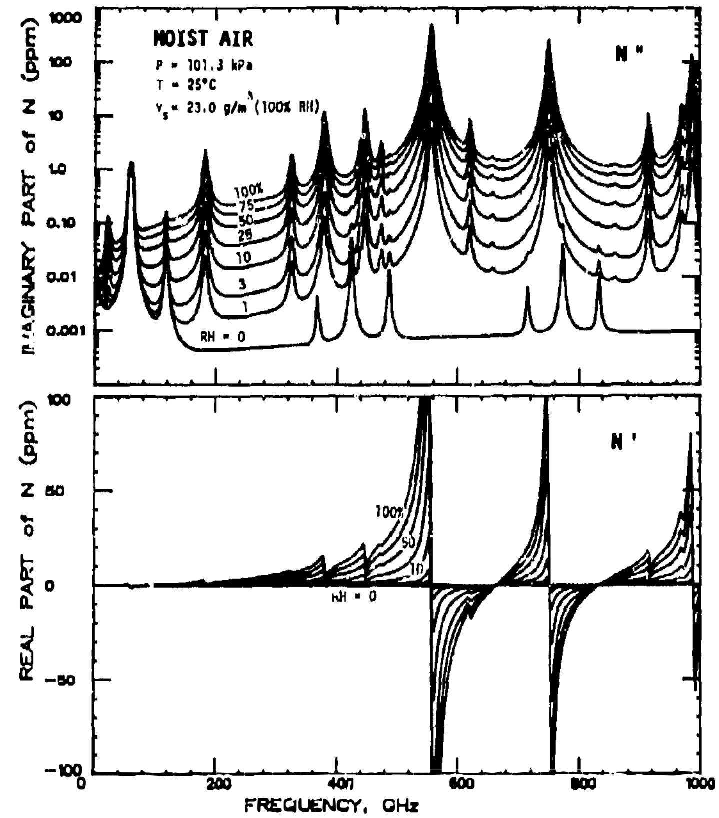

Fig. 1. Atmospheric dispersive refractivity N = N'(f) + iN"(f) over the frequency range from 0 to 1000 GHz for a sea level condition (P,T) at various relative humidities (U).

α

τ

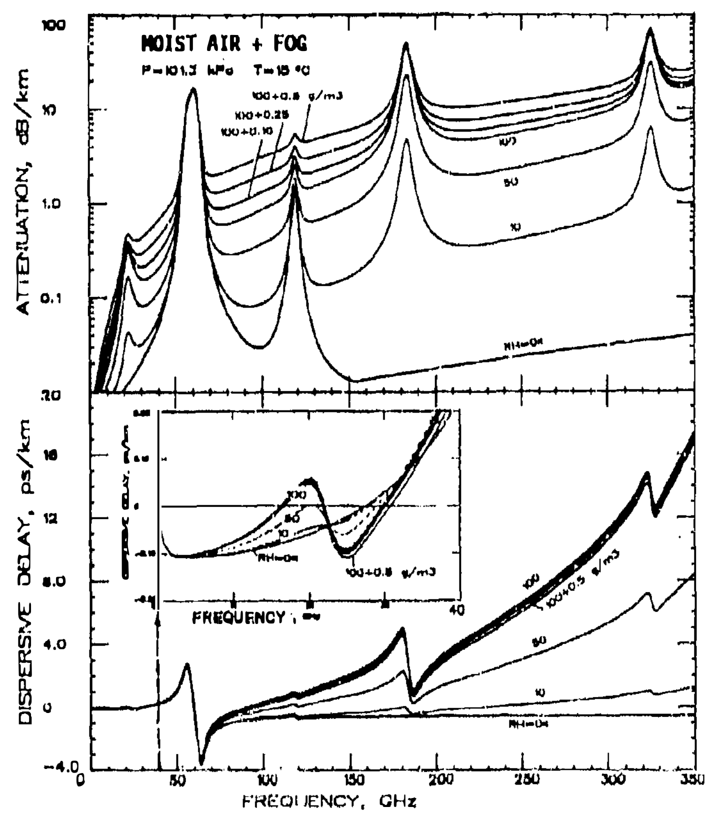

Fig. 2. Attenuation (α) and delay (τ) rates for fog cases (W = 0.1, 0.25, 0.5 g/m³) added to a saturated sea level condition. Also shown are dry air (0 %RH) and moist air (10, 50 %RH) characteristics.

The parameters in (16) are best fits to measured permittivity data reported for frequencies up to 1000 GHz over a temperature range from -10 to 30°C.

2.7 MPM Examples

Examples for a sea level condition exhibit spectra at various relative humidities (U = 0 to 100 %RH) in Figure 1. Molecular resonance absorption can be recognized in the 60-GHz band, at 119 GHz, and higher due to O_2, as well as around 22, 183 GHz, and higher due to H_2O. Across the spectrum one notices more or less transparent window ranges separated by molecular resonance peaks. Above 120 GHz, relative humidity (7) is a key variable to describe the dominating water vapor effects of absorption and dispersive refractivity.

Systems designed for the millimeter-wave (90 - 350 GHz) range offer an attractive alternative to electro-optical schemes when operation has to be assured during periods of optical obscuration. Water droplet effects (15) of MPM are added to the state of saturated (U = 100 %RH) air by specifying a concentration W. Typical attenuation and delay rates due to fog are displayed in Figure 2.

3. THE MZM MODEL

The mesosphere lies between the stratosphere and thermosphere from somewhat above 30 km in altitude to about 100 km. Air is dry and the environmental parameters are pressure P (1.2 to $3 \cdot 10^{-5}$ kPa) and temperature T (-2 to -87°C) taken from the U.S. Standard Atmosphere 76 [13]. Oxygen line absorption is strong enough to affect radio propagation. Because the pressure is low, the lines are very sharp and new phenomena appear due to the *Zeeman* effect. The geomagnetic field (magnetic flux density B_0 can vary from 22 to 65 μT) splits each line into a number of sublines, and, furthermore, how these sublines react to an electromagnetic field depends on its polarization state. Over a few megahertz around the line centers, the medium is anisotropic, making radio waves subject to polarization discrimination and Faraday rotation. The physical reasons for this behavior and possible applications are discussed in references [9]-[12]. This background led to MZM, which shows how wave propagation in the mesosphere can be handled [2].

3.1 Oxygen Line Properties As Influenced By The Geomagnetic Field (Zeeman Effect)

The O_2 molecule interacts with radiation via its magnetic dipole moment. Rotational energy levels of the linear molecule have approximate values given by the formula BK(K+1), where B is related to the moment of inertia of the molecule and the "quantum number" K is an odd integer. The microwave lines originate from the fine structure of the K levels caused by the electron spin. For each K, the "total angular momentum" quantum number takes on values J = K-1, K, K+1. Transitions can take place between the K and K+1 levels and between the K and K-1 levels and are labeled the K^+ and K^- absorption lines, respectively.

The program MZM is relevant only ±10 MHz around isolated line centers $\nu_0(K^\pm)$ but operates in principle over ±250 MHz. Each line strength and width is calculated with (12a,b). Center frequencies ν_0 and spectroscopic parameters a_1, a_2, and a_3 are listed in Table 1 for 40 O_2 absorption lines. Most of the 60-GHz lines are generally separated by about 500 MHz; since the line width above 30 km is 20 MHz or less, each line is well isolated. There are four cases where $K^\pm$ lines are separated by only about 100 MHz. These lines must be treated as "doublets" to account below h ≈ 50 km for overlapping contributions.

Pressure decreases with altitude and the O_2 width approaches the *Doppler* width (ν_0 in GHz)

$$\gamma_D = 1.096 \cdot 10^{-6} \nu_0 / \theta^{1/2} \quad \text{GHz}, \tag{17}$$

which is associated with a *Gaussian* shape function. The transition between pressure and thermal broadening is handled theoretically by a *Voigt* line shape (convolution of Lorentz and Gauss functions) [12]. Following [14], it is adequate to retain the Lorentz shape function (i.e., first term of equation 12) and to suppose that the width γ_i (12b) is replaced by

$$\gamma_h = 0.535\gamma + (0.217\gamma^2 + \gamma_D^2)^{1/2} \quad \text{GHz}. \tag{18}$$

Each of the fine structure J-levels is degenerate since the corresponding states have random azimuthal motion. The quantum number M of azimuthal momentum can be any integer from -J to +J. When the O_2 molecule is subjected to a static magnetic field, a force is acting on the internal magnetic dipole. The resulting precession about the field affects the rotational energy in a manner directly related to the azimuthal quantum number M. The level then splits into 2J+1 new levels. This elimination of degeneracy is called the *Zeeman* effect.

There are stringent selection rules for transitions between the many energy levels. When J changes by one, then simultaneously M can either remain fixed or else also change by one. Furthermore, each of those transitions can arise because of interaction with only one component of the electromagnetic field. The line components obtained when M is unchanged are called the π components and arise from interaction with a magnetic field vector that is linearly polarized in the direction of $\underline{B}$. When M changes by ±1, the σ^+ or σ^- components are excited by a magnetic field vector which is circularly polarized in the plane perpendicular to $\underline{B}$. The σ^+ (σ^-) components arise from a right (left) circularly polarized field. This anisotropic behavior is explained by noting that circularly polarized forces along the axis of rotation ought to change the azimuthal motion. Each set of components of the K^+ line contains 2K+1 sublines, while the K^- line contains 2K-1 sublines.

The line center frequency of a single Zeeman component is given by

$$\nu_0^{\pm} = \nu_0 + 28.03 \cdot 10^{-6} \eta_M B_0 \quad \text{GHz} \tag{19}$$

where ν_0 is the center frequency of the unsplit line, B_0 is in μT, and $\eta_M \leq \pm 1$ is a coefficient that depends on $K^\pm$, M, and ΔM. A geomagnetic field of 50 μT spreads the Zeeman components over about ν_0 ± 1.5 MHz.

Table 1. Line Frequencies ν_0 and Spectroscopic Coefficients $a_{1,2,3}$ for Microwave Transitions of O_2 in Air

K±	ν_0	a_1	a_2	a_3
	GHz	kHz/kPa $\times 10^{-6}$		GHz/kPa $\times 10^{-3}$
39−	49.962257	0.34	10.724	8.50
37−	50.474238	0.94	9.694	8.60
35−	50.987749	2.46	8.694	8.70
33−	51.503350	6.08	7.744	8.90
31−	52.021410	14.14	6.844	9.20
29−	52.542394	31.02	6.004	9.40
27−	53.066907	64.10	5.224	9.70
25−	53.595749	124.70	4.484	10.00
23−	54.130000	228.00	3.814	10.20
21−	54.671159	391.80	3.194	10.50
19−	55.221367	631.60	2.624	10.79
17−	55.783802	953.50	2.119	11.10
1+	56.264775	548.90	0.015	16.46
15−	56.363389	1344.00	1.660	11.44
13−	56.968206	1763.00	1.260	11.81
11−	57.612484	2141.00	0.915	12.21
9−	58.323877	2386.00	0.626	12.66
3+	58.446590	1457.00	0.084	14.49
7−	59.164207	2404.00	0.391	13.19
5+	59.590983	2112.00	0.212	13.60
5−	60.306061	2124.00	0.212	13.82
7+	60.434776	2461.00	0.391	12.97
9+	61.150560	2504.00	0.626	12.48
11+	61.800154	2298.00	0.915	12.07
13+	62.411215	1933.00	1.260	11.71
3−	62.486260	1517.00	0.083	14.68
15+	62.997977	1503.00	1.665	11.39
17+	63.568518	1087.00	2.115	11.08
19+	64.127767	733.50	2.620	10.78
21+	64.678903	463.50	3.195	10.50
23+	65.224071	274.80	3.815	10.20
25+	65.764772	153.00	4.485	10.00
27+	66.302091	80.09	5.225	9.70
29+	66.836830	39.46	6.005	9.40
31+	67.369598	18.32	6.845	9.20
33+	67.900867	8.01	7.745	8.90
35+	68.431005	3.30	8.695	8.70
37+	68.960311	1.28	9.695	8.60
39+	69.489021	0.47	10.720	8.50
1−	118.750343	945.00	0.009	16.30

Table 2. Relative Shift (η_M) and Strength (ξ_M) Factors for the Zeeman Components

Zeeman transitions	K^+ - Lines		K^- - Lines	
	$\eta_M(K)$	$\xi_M(K)$	$\eta_M(K)$	$\xi_M(K)$
	$M=-K,-K+1,\ldots,K$		$M=-K+1,-K+2,\ldots,K-1$	
π ($\Delta M=0$)	$\frac{M(K-1)}{K(K+1)}$	$\frac{3((K+1)^2-M^2)}{(K+1)(2K+1)(2K+3)}$	$\frac{M(K+2)}{K(K+1)}$	$\frac{3(K^2-M^2)}{K(2K+1)(2K-1)}$
σ^+ ($\Delta M=1$)	$\frac{M(K-1)-K}{K(K+1)}$	$\frac{3(K-M+1)(K-M+2)}{4(K+1)(2K+1)(2K+3)}$	$\frac{M(K+2)-1}{K(K+1)}$	$\frac{3(K-M+1)(K-M)}{4K(2K+1)(2K-1)}$
σ^- ($\Delta M=-1$)	$\frac{M(K-1)+K}{K(K+1)}$	$\frac{3(K+M+1)(K+M+2)}{4(K+1)(2K+1)(2K+3)}$	$\frac{M(K+2)+1}{K(K+1)}$	$\frac{3(K+M+1)(K+M)}{4K(2K+1)(2K-1)}$

Each of the three sets of Zeeman components leads to a refractivity spectrum,

$$N_i(f) = \Sigma_M S \xi_M F_M(f) \ , \tag{20}$$

where the subscript i = o, +, - designates π and $\sigma^{\pm}$-components, respectively; the function F_M is a single Lorentzian [first term of (12), δ = 0, and f/ν_0 = 1] plus line strength S and line width γ_h, both independent of M, and equal to the values given by (12a) and (18). The scheme to calculate the coefficients η_M and ξ_M for the individual Zeeman components of each $K^{\pm}$ line is given in Table 2 [2],[12], based on the work by Lenoir [10]. Note that $\Sigma_M\xi_M$ equals 1 in the case of N_o and 1/2 for the other two ($N_\pm$). When B_0 = 0 in (19) all the functions F_M are equal and the terms in (20) add so that $2N_+ = 2N_- = N_o = N_L$.

Magnitude and direction of the geomagnetic vector $\underline{B}$ are calculated with the geocentric model MAGFIN, which is updated with 1985 coefficients [15]. To allow for geodetic input coordinates (LAT_itude, LON_gitude, and ALT_itude above sea level), a small correction to latitude and altitude is applied to account for the flattening (1/298.25) of the Earth. It follows that path lengths traced through the mesosphere in N-S directions are slightly less than those in E-W directions (see Fig. 6).

The three spectra N_i are components of the constitutive properties in the mesosphere. Since it is the paramagnetic properties of oxygen that bring about the absorption lines, it is the magnetic permeability that is affected. The relative permeability of an anisotropic medium is formally a tensor of rank 2,

$$\mu_r = I + 2N \tag{21}$$

assuming N is on the order of 10^{-6}, and I is the unit tensor of a coordinate system for the basis $|\underline{e}_x \ \underline{e}_y \ \underline{e}_z|$ and N is represented as a 3x3 matrix. When the z-axis is pointing in direction $\underline{e}_z = \underline{e}_0$ of the geomagnetic vector $\underline{B}$, we have

$$N = \begin{pmatrix} N_+ + N_- & -i(N_+ - N_-) & 0 \\ i(N_+ - N_-) & N_+ + N_- & 0 \\ 0 & 0 & N_o \end{pmatrix} , \tag{22}$$

where N_o, N_+, N_- are complex-valued functions of frequency expressed by (20). The shape of these functions is illustrated for an example in Figure 3.

3.2 Basic Equations For Plane-Wave Propagation

The tensor N may be introduced in Maxwell's equations in the form of (22) and a plane-wave solution formulated [2]. Such solution takes the form of (5). The electric field strength $\underline{E}$ is a 2-dimensional vector in the xy-plane and N_2 is a 2x2 submatrix of N. The real unit vectors $\underline{e}_x$, $\underline{e}_y$ define the plane of polarization which combines with $\underline{e}_z$, the direction of propagation, to form a righthanded orthogonal triad.

The refractivity tensor N was represented as a 3x3 matrix of the anisotropic medium. It depends for its definition on $\underline{e}_0$, the unit vector in the direction of the geomagnetic field. To obtain the 2x2 matrix N_2 acting on the plane of polarization of the radio wave $\underline{E}(z)$, we let ϕ be the angle between the geomagnetic field and the direction of propagation, that is, between $\underline{e}_0$ and $\underline{e}_z$. Then the rotation of the "old" coordinate system with basis $|\underline{e}_x' \ \underline{e}_y' \ \underline{e}_0|$, in which N is represented as in (22), and the "new" system with basis $|\underline{e}_x \ \underline{e}_y \ \underline{e}_z|$ gives N_2.

A physically natural approach was to treat refractivity and its propagation effects as associated with the magnetic wave vector $\underline{H}$, which was then changed via the impedance of free space to the corresponding electric field vector $\underline{E}$. The vector $\underline{E}$ is not orthogonal to $\underline{H}$ but the discrepancy is only of order N. It follows that the refractivity matrix in (5) is given by [2]

$$N_2 = \begin{pmatrix} N_o\sin^2\phi + (N_+ + N_-)\cos^2\phi & -i(N_+ - N_-)\cos\phi \\ i(N_+ - N_-)\cos\phi & N_+ + N_- \end{pmatrix} . \tag{23}$$

3.3 Characteristic Waves

The computation of the exponential in (5) may be carried out using the technique of spectral decomposition of the square matrix N_2 [16]. We look for complex numbers ρ (the "eigenvalues") and vectors $\underline{v}$ (the "corresponding eigenvectors") that satisfy

$$N_2 \ \underline{v} = \rho \ \underline{v} \ . \tag{24}$$

To solve (24), we first treat the scalar equation (the "characteristic equation") [2]

$$\det(\rho I - N_2) = 0 \ . \tag{25}$$

Since these are 2x2 matrices, this equation is quadratic in ρ and there should be two solutions ρ_1 and ρ_2. Given these numbers, it is possible to find the corresponding eigenvectors $\underline{v}_1$ and $\underline{v}_2$. Whenever the initial field $\underline{E}_0$ equals an eigenvector, then (5) becomes

$$\underline{v}_{1,2}(z) = \exp[ikz(1 + \rho_{1,2})] \ \underline{v}_{1,2} \ . \tag{26}$$

The two vector functions $\underline{v}_1(z)$ and $\underline{v}_2(z)$ are plane-wave solutions to Maxwell's equation called *characteristic waves*. They have the property that, while they may change in amplitude and phase, they always retain their original appearance and orientation. The two eigenvectors are linearly independent, and for any initial field we may find complex numbers E_1 and E_2, so that

$$\underline{E}_0 = E_1 \ \underline{v}_1 + E_2 \ \underline{v}_2 \ . \tag{27}$$

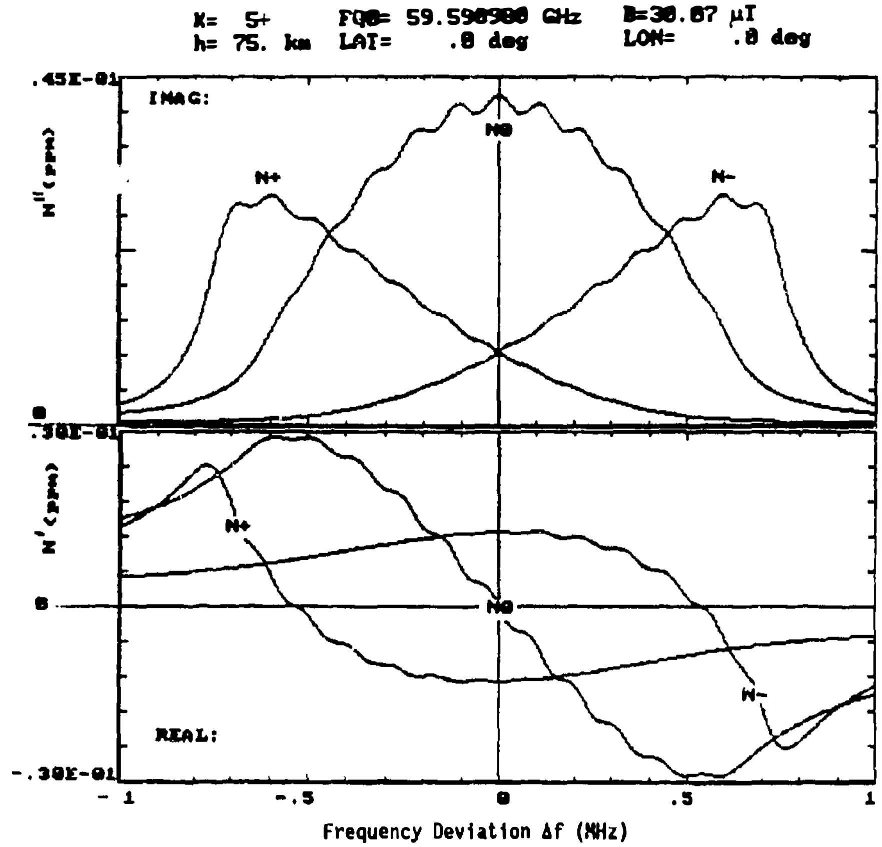

Fig. 3. Refractivity components N_0, N_+, and N_- (ppm) in the vicinity (Δf= ±1 MHz) of the K = 5^+ line for h = 75 km at LAT=0° (equator) and LON=0° (Greenwich) where the flux density is B_0 = 30.07 μT.

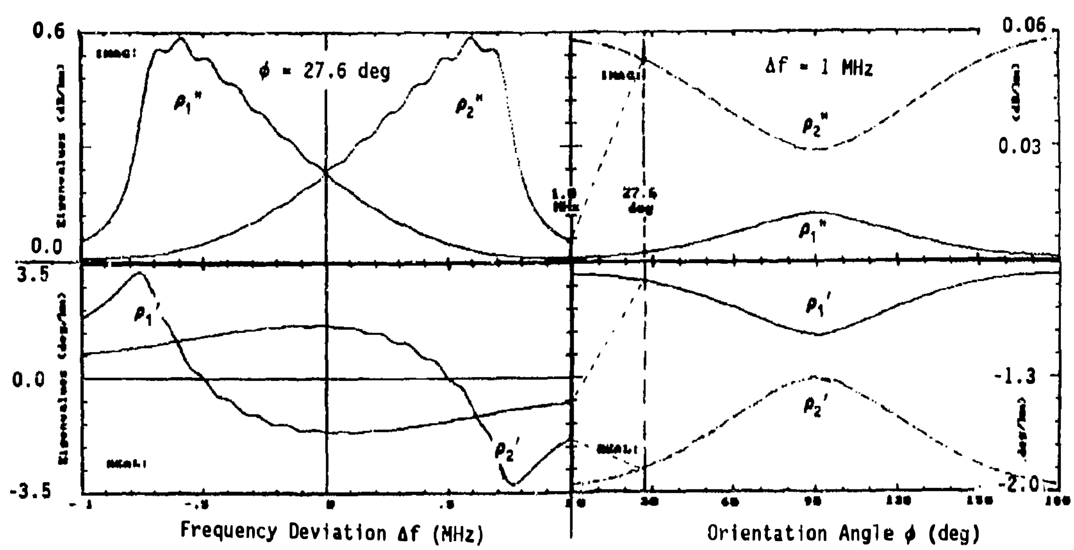

Fig. 4. Complex eigenvalues ρ_1 and ρ_2 for the 5^+ line at h=75 km and LAT=0°, LON = 0° (*IMAG* in dB/km, *REAL* in deg/km): (a) around the line center (Δf = ±1 MHz) at an orientation angle φ = 27.6 ° and (b) for orientation angles φ = 0 to 180° at a frequency deviation Δf = +1 MHz.

Then the exponential in (5) becomes

$$\underline{E}(z) = e^{ikz}[E_1\exp(ikz\,\rho_1)\,\underline{v}_1 + E_2\exp(ikz\,\rho_2)\,\underline{v}_2] \quad . \tag{28}$$

The field vector is now represented as a linear combination of the two characteristic waves.

The eigenvalues, ρ_1 and ρ_2, have the same order of magnitude as the N_i values and have positive, generally differing, imaginary parts; hence, as z increases, $\underline{E}(z)$ decreases exponentially and one of the two components drops faster than the other. After some distance z, $\underline{E}(z)$ approaches the appearance of the remaining characteristic wave. Also, the real parts of the eigenvalues can differ. The two characteristic waves travel at different speeds through space and the phase relation between the two components in (28) varies continuously. In the process, the ellipse of polarization exhibits a "Faraday rotation."

Eigenvalues and eigenvectors are computed with

$$\rho_1\rho_2 = \det(\underline{N}_2) = 4N_+N_-\cos^2\phi + N_o(N_+ + N_-)\sin^2\phi$$

and

$$\rho_1 + \rho_2 = \mathrm{trace}(\underline{N}_2) = 2(N_+ + N_-) + (N_o - N_+ - N_-)\sin^2\phi \quad , \tag{29}$$

from which ρ_1 and ρ_2 may be found. These complex-valued functions depend on frequency and orientation angle as demonstrated by the example in Figure 4. Let us suppose that ρ is one of these two and that we seek the corresponding eigenvector $\underline{v}$. Its components have the values v_x, v_y, so that (24) becomes a set of two equations in these two unknowns. The second of these equations is

$$i(N_+ - N_-)\cos\phi\; v_x + (N_+ + N_-)v_y = \rho\; v_y \tag{30}$$

and one solution is

$$v_x = \rho - N_+ - N_- \qquad \text{and} \qquad v_y = i(N_+ - N_-)\cos\phi \quad . \tag{31}$$

Since ρ is an eigenvalue, the first equation is also satisfied. The two eigenvectors, v_1 and v_2, of (27) are usually not orthogonal.

A special case occurs when $\phi = 0$. The solutions to (29) are $\rho_1 = 2N_+$ and $\rho_2 = 2N_-$, and when these are inserted into (31), the corresponding eigenvectors are, respectively, right circularly polarized and left circularly polarized and the z-axis is the direction of the geomagnetic field. When $\phi = \pi/2$, the eigenvalues are N_o and $N_+ + N_-$, and the corresponding eigenvectors are linearly polarized with the $\underline{E}$ vector pointing respectively along the x-axis and along the y-axis.

3.4 Polarization And Stokes Parameters

The polarization of a radio-wave field changes as it propagates through the Zeeman medium and we have to quantify the polarization. The vector $\underline{E}$ (5) describes an "ellipse of polarization" that can be characterized by *Stokes* parameters. These are discussed in many texts (e.g., [17]) and here we summarize only some of their attributes.

Let $\underline{E}$ lie in the x,y-plane and E_x, E_y be the complex-valued field components. Then the four Stokes parameters $g_{0,1,2,3}$ are real numbers given by

$$g_0 = |E_x|^2 + |E_y|^2 \qquad g_1 = |E_x|^2 - |E_y|^2 \qquad g_2 = 2\,Re[E_x^*\,E_y] \qquad g_3 = 2\,Im[E_x^*\,E_y] \tag{32}$$

where the star indicates the complex conjugate. We note that g_0 is positive and equals the total field strength and recognize that

$$g_0^2 = g_1^2 + g_2^2 + g_3^2.$$

In a three-dimensional space with g_1, g_2, g_3 axes, the Stokes parameters of a field vector lie on the surface of a sphere of radius g_0. This is the *Poincaré* sphere and provides a geometric picture of the field vector polarization. Given the Stokes parameters, we can write for some phase angle ψ, that

$$E_x = [(g_0 + g_1)/2]^{1/2}e^{i\psi} \qquad \text{and} \qquad E_y = ((g_2 + ig_3)/[2(g_0 + g_1)]^{1/2})e^{i\psi} \quad . \tag{33}$$

The vector $\underline{E}$ determines within the phase angle ψ the Stokes parameters and vice versa. Since the absolute phase of the field remains undefined, the Stokes parameters represent all the useful information for the field. What relates the parameters directly to the ellipse of polarization is the representation of the Poincaré sphere in spherical coordinates

$$g_1 = g_0\cos2\tau\,\cos2\delta \;, \qquad g_2 = g_0\cos2\tau\,\sin2\delta \;, \qquad g_3 = g_0\sin2\tau \;. \tag{34}$$

It turns out that δ $(0 \le \delta < \pi)$ is the angle between the major axis of the ellipse and the x-axis, while $\tan\tau = \pm b/a$ $(-\pi/4 \le \tau \le \pi/4)$, where a and b are the major and minor semiaxes and the sign is chosen according to the sense of rotation. Thus the four Stokes parameters provide a complete description of the polarization.

If one limits the discussion to polarization, the Stokes parameters can be normalized by dividing them all by g_0 and the Poincaré sphere has unit radius. Treating this sphere as a globe, the northern hemisphere and the north pole correspond to right-hand polarization and right circular polarization (RC), while the southern hemisphere and the south pole correspond to left-hand polarization and to left circular polarization (LC). The equator corresponds to linear polarization with "east" at $(g_1,g_2,g_3) = (1,0,0)$ corresponding to polarization along the x-axis (HL) and "west" $(-1,0,0)$ to polarization along the y-axis (VL).

An alternate way to describe polarization uses the complex number p defined as a ratio of the two field components [18]. From (33) one obtains

$$p = E_y/E_x = (g_2 + ig_3)/(g_0 + g_1) \ , \tag{35}$$

(when $E_x = 1$ then $p = |E_y|e^{i\varphi}$) and, when the Stokes parameters are normalized,

$$g_1 = (1 - |p|^2)/(1 + |p|^2) \quad , \quad g_2 + ig_3 = 2p/(1 + |p|^2) \ . \tag{36}$$

The real p-axis corresponds to linear, the upper half-plane to right-hand, and the lower half-plane to left-hand polarizations. The points $p = i$, $-i$, 0, and ∞ correspond respectively to right circular, left circular, linear along the x-axis, and linear along the y-axis polarizations. The advantage of notation (35) is the fact that the seemingly complicated polarization description has been reduced to a single number. The disadvantage is a lack of symmetry between small values of p (near $g_1 = 1$) and large values (near $g_1 = -1$).

3.5 MZM Model Features And Propagation Examples

Generally, a radio wave is defined as a linear combination of the two characteristic waves (28). Horizontal and vertical field components [E_x(HZE) = 1, $p = E_y(VTE) = |E_y|e^{i\varphi}$, where φ(POL) is the polarization angle (35)], or a matching set of Stokes parameters [$g_{1,2,3}$ normalized to $g_0 = 1$ and $\phi = 0$ (33)] describe the polarization state. Typically, the **imaginary** parts (expressed in dB/km) of ρ_1 and ρ_2 differ (see Fig. 4), favoring after some propagation distance the characteristic wave with the lower value; simultaneously, different real parts (in deg/km) affect the polarization angle φ. As a consequence, the polarization ellipse changes its axial ratio and "Faraday"-rotates approaching the polarization state of the dominant characteristic wave.

The mesospheric model MZM gives a solution to the problem introduced by (5). It analyzes the geomagnetic Zeeman effect of O_2 microwave lines to predict anisotropic propagation of polarized radio waves at about ±10 MHz (Δf) from the line centers. Numerous input parameters are specified:

- frequency, defined as deviation from a particular ($K^{\pm}$) O_2 line center ($\Delta f = \nu_0 \pm f$)
- geodetic coordinates of the location where the wave originates (LAT_itude, LON_gitude, and ALT_itude)
- environmental parameters (pressure P and temperature T)
- geomagnetic field vector $\underline{B}$ [components B_n (north), B_e (east), B_u (up)] and flux density B_0
- polarization state of the launched plane radio wave [p (HZE=1, VTE) and φ(POL)]
- direction and elevation angle [ϕ (AZI_muth, ELE_vation)] of the launched wave

The $K^{\pm}$ = 5+ line (ν_0 = 59.590983 GHz) has been chosen as an example. Two cases are discussed:

a) in a homogeneous atmosphere for given LAT, LON, and ALT(75 km), a radio wave propagates north at the frequency ν_0 + 1 MHz covering a distance z of up to 1000 km, and

b) at a location LAT, LON, ALT(100 km), a wave enters the inhomogeneous atmosphere, heads in either N, E, S, or W directions, descends to an altitude of 75 km, and then exits again at the 100 km level.

In the first case, path attenuation A and polarization state are followed along. Propagation effects are shown in Figure 5 as a function of distance z for a case where h (ALT), $\underline{B}$ (LAT, LON), and ϕ (AZI, ELE) are given to determine $\rho_1(\underline{v}_1)$ and $\rho_2(\underline{v}_2)$. At the frequency $\nu_0(5^+)$ + 1 MHz, two initial polarizations are propagated along a path ranging at h = 75 km to a length of up to 1000 km. Results at z = 1000 km are

Initial Polarization	A (dB)	Final Polarization			Figure
45°L	10.9	HZE=1,	|VTE|=1.04,	POL=87.4°	5
LC	39.5	1	1.37	70.0°	5
RC	8.0	1	1.04	88.0°	-
HL	11.2	1	1.03	88.2°	-
VL	10.8	1	1.05	87.8°	-

Computations are more complicated for the second case, where a tangential path from outer space reaches a minimum height, h_t = 75 km. Starting at h = 100 km in a given direction (AZI) under an elevation angle, ELV = - 5.1°, a radio ray was traced through a homogeneous path cell via the coordinates LAT, LON, and ALT. Geodetic locations were transformed into geocentric coordinates to compute $\underline{B}$, ϕ, and path increments Δz for 1-km height intervals; then a numerical integration was performed whereby the anisotropic behavior of each cell was evaluated analogously to the case exemplified in Fig. 5. The final polarization after traversing one cell served as starting polarization for the next. Total path attenuations A as a function of frequency deviation (ν_0 ± 4 MHz), initial polarization, and direction are given. Path attenuations for three different initial polarizations and four propagation directions are plotted in Figure 6 as a function of the frequency deviation Δf. Each curve represents the integration over fifty (100 → 75 → 100 km) 1-km thick cells performed at 100 frequencies between ν_0 ± 4 MHz. The path attenuations A(dB) at Δf(DFQ) = 1 MHz are

AZI	Direction	HL	VL	Ratio	RC	LC	Ratio
0°	N	6.4	6.7	1.05	3.5	27.6	7.89
90°	E	13.5	8.7	1.55	12.6	9.1	1.39
180°	S	7.1	7.6	1.07	22.7	4.4	5.16
270°	W	11.9	8.5	1.40	8.5	12.3	1.45

4. CONCLUSIONS

Two parametric models of atmospheric refractivity N (1) have been discussed. Wave propagation described by (2) uses the isotropic model of N(f; P,T,U; W), which is organized by MPM in five modules to control over 500 parameters. It was developed for applications in areas such as telecommunications, radar, remote sensing, and radio astronomy, which operate in the neutral atmosphere between 1 GHz and 1 THz. For MPM, various shortcomings remain (e.g., empirical nature of H_2O continuum absorption and missing trace gas spectra). The physical origin of the water vapor spectrum in MPM is still not fully understood. Especially, the lack of a theoretical basis for the e^2-term of continuum absorption (14) is a source of concern. Its largely empirical origin can introduce modeling errors when predicting transmission effects in atmospheric window ranges. Research to uncover the true nature of the millimeter-wave water vapor continuum poses a challenge.

The anisotropic model of $N_z(K^{\pm},\Delta f;\ P,T;\ \underline{E};\ \underline{B};\ \phi)$ is applied in MZM to a special propagation case that is described by (5) to treat the Zeeman effect of the O_2 lines listed in Table 1. The model predicts the transmission of polarized, plane waves through a spherically stratified (30 - 100 km) mesosphere at frequencies in close proximity of line center frequencies. For MZM, the experimental confirmation of the anisotropic geomagnetic Zeeman effect remains to be realized.

Programs for MPM and MZM were written to run efficiently on desk-top microcomputer (diskettes may be requested from ITS). Validation, error checking of predictions, and incorporation of new research results will continue to be critical and time consuming tasks.

5. REFERENCES

[1] Liebe, H. J.: MPM - an atmospheric millimeter-wave propagation model, *Int. J. IR and MM Waves*, 10(6), 631-650, 1989.

[2] Hufford, G. H. and H. J. Liebe: Millimeter-wave propagation in the mesosphere, NTIA Report 89-249, U.S. Dept. Commerce, Boulder, CO, September 1989.

[3] Liebe, H. J.: An updated model for millimeter wave propagation in moist air, *Radio Sci.*, 20(5), 1069-1089, 1985.

[4] Danese, L. and R. B. Partridge: Atmospheric emission models: confrontation between observational data and predictions in the 2.5 - 300 GHz frequency range, *Astrophys. J.*, 342, 604-615, 1989.

[5] Rosenkranz, P. W.: Interference coefficients for overlapping oxygen lines in air, *J. Quant. Spectr. Rad. Transf.*, 39(4), 287-297, 1988.

[6] Rosenkranz, P. W.: Chapter 2 in Atmospheric Remote Sensing By Microwave Radiometry (M. A. Janssen, ed.), Wiley-Interscience, New York, N.Y., 1989.

[7] Liebe, H. J. and D. H. Layton: Millimeter-wave properties of the atmosphere -- laboratory studies and propagation modeling, NTIA-Report 87-224, U.S. Dept. Commerce, Boulder, CO., October 1987.

[8] Liebe, H. J., T. Manabe, and G. H. Hufford: Millimeter-wave attenuation and delay rates due to fog/cloud conditions, *IEEE Trans. Ant. Prop.*, AP-37(12), in press, 1989.

[9] Townes, C. H. and A. L. Schawlow: Microwave Spectroscopy (Chapter 11), McGraw-Hill, New York, N.Y., 1955.

[10] Lenoir, W. B.: Microwave spectrum of molecular oxygen in the mesosphere, *J. Geophys. Res.*, 73, 361-376, 1968.

[11] Rosenkranz, P. W. and D. H. Staelin: Polarized thermal emission from oxygen in the mesosphere, *Radio Sci.*, 23(5), 721-729, 1988.

[12] Liebe, H. J.: Modeling attenuation and phase delay of radio waves in air at frequencies below 1000 GHz, *Radio Sci.*, 16(6), 1183-1199, 1981.

[13] COESA, U.S. Committee on Extension to the Standard Atmosphere: U.S. Standard Atmosphere 76, NOAA-S/T 76-1562; U.S. Gov. Printing Office, Washington, D.C., 1976.

[14] Olivero, J. J. and R. L. Longbothum: Empirical fits to the Voigt line width -- a brief review, *J. Quant. Spectr. Rad. Transf.*, 17, 233-236, 1977.

[15] Barraclough, D. R.: International Geomagnetic Reference Field revision 1985, *Pure and Appl. Geophys.*, 123, 641-645, 1985.

[16] Moler, C. and C. Van Loan: Nineteen dubious ways to compute the exponential of a matrix, *SIAM Rev.*, 20, 801-836, 78.

[17] Born, M. and E. Wolf: Principles of Optics (Section 1.4), Pergamon Press, New York, N.Y., 1959.

[18] Beckmann, P.: The Depolarization of Electromagnetic Waves, Golem Press, Boulder, CO., 1968.

6. ACKNOWLEDGMENTS

The authors acknowledge with gratitude the programming help provided by A. S. Katz in setting up MZM. Preparation of this paper was supported in part by the Naval Ocean Systems Center (Ref: RA35 G80).

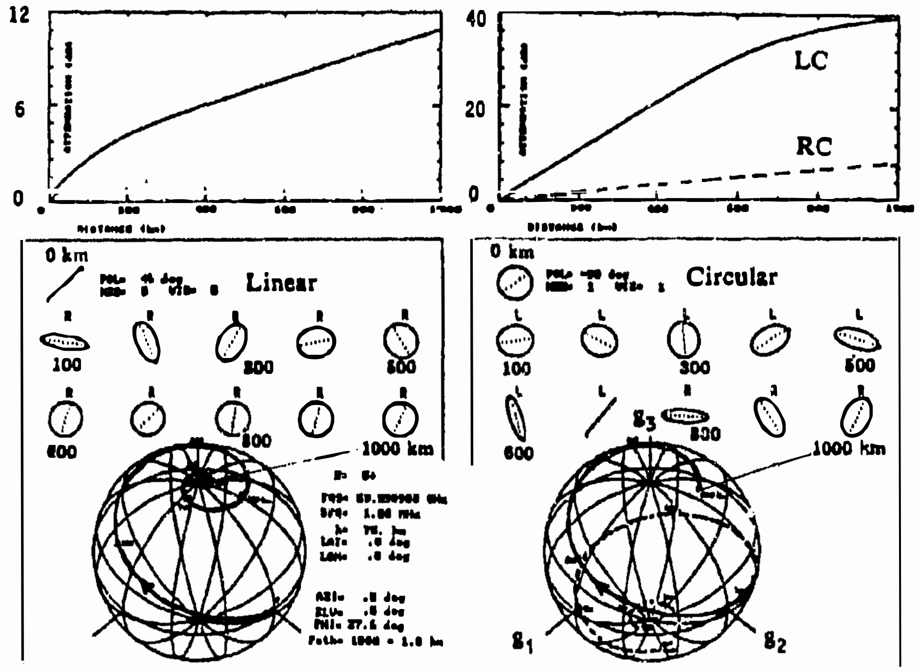

Fig. 5. Attenuation, Faraday rotation, and polarization state (Stokes parameters $g_{1,2,3}$ on Poincaré sphere) for initially linear (45°L) and left-circular (LC) polarized radio waves propagating a distance of 1000 km at h = 75 km horizontally (ELV = 0°) in the north direction (AZI = 0°) under the computed orientation angle ϕ(PHI) = 27.6° at a frequency f = $\nu_0(5^+)$ + 1 MHz.

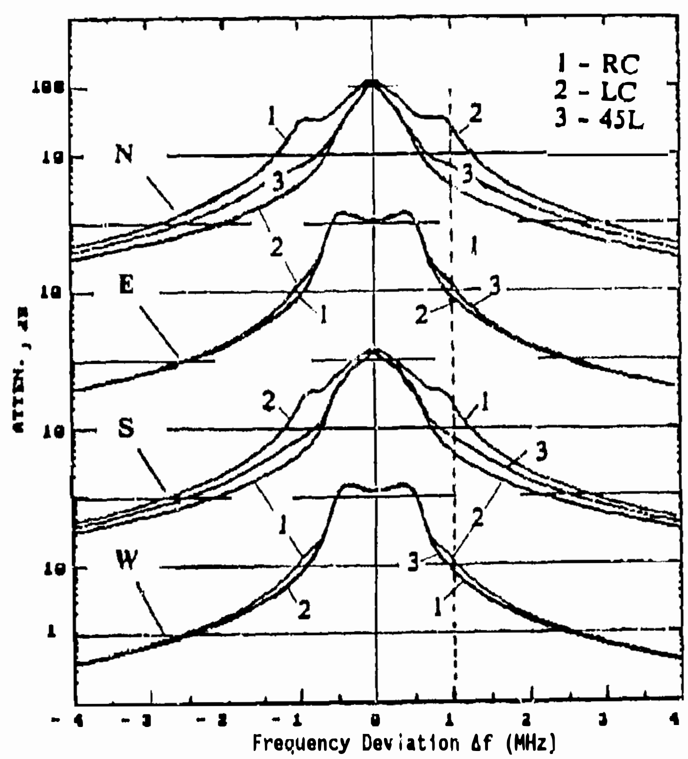

Fig. 6. Cumulative path attenuation A for tangential path through the U.S. Std. Atm. [13] in the vicinity [Δf(DFQ) = ±4 MHz] of the K=5⁺ line. The radio wave enters the atmosphere at LAT=0°, LON=0°, and h(ALT)=100 km with an elevation angle ELV=-5.1°, propagates in either N, E, S, or W directions (AZI=0°, 90°, 180°, 270°), approaches a tangential height of 75 km, and leaves the atmosphere at h = 100 km. Path lengths: z_{total} = 1129 km for N or S, and 1140 km for E or W directions; initial polarizations: right-hand circular (RC), left-hand circular (LC), and 45° linear (45L).

DISCUSSION

J. SELBY

You showed good agreement between your calculations of atmospheric attenuation and some field measurements for your H_2O and O_2 line parameters and your H_2O continuum. How do your molecular line parameters and the H_2O continuum compare with those of AFGL (in HITRAN 86 and FASCOD 2)?

AUTHOR'S REPLY

I showed results from two experiments that confirmed MPM89 [1] predictions of atmospheric water vapor attenuation:

a. about 1200 data (0.1-1.2 dB/km) from field measurements performed at 96.1 GHz (2-20 g/m^3 H_2O, 5-35°C, 98 kPa) [Manabe et al., IEEE Trans AP-37(2), Feb 1989]; and

b. about 180 data (2-20,000 dB/km) reported between 175 and 950 GHz for the monomer (proportional to ep) spectrum at 7.5 g/m^3, 20°C, 101 kPa plus 35 data (0.3-1.2 dB/km) reported between 210 and 440 GHz to support a theoretical dimer spectrum as H_2O continuum, which is proportional to $b_e e^2$ (see equation (14) and reference [7]); [Furashov et al., IEE Conf. Publ. 301, 310-11, ICAP 89].

MPM89 uses from the AFGL HITRAN code only the line strength parameters of 30 H_2O lines -- all other spectroscopic information either originated from our laboratory work or the references given in [1].